Composites Part A 128 (2020) 105646

Contents lists available at ScienceDirect

Composites Part A

journal homepage: www.elsevier.com/locate/compositesa

Swarm intelligence integrated micromechanical model to investigate thermal conductivity of multi-walled carbon nanotube-embedded cyclic butylene terephthalate thermoplastic nanocomposites

Seong Yun Kim[a], Ji-un Jang[a], Bezawit F. Haile[b], Min Wook Lee[c], Beomjoo Yang[d,*]

[a] Division of Polymer-Nano & Textile Engineering, Chonbuk National University, 567 Baekje-daero, Deokjin-gu, Jeonju, Jeonbuk 54896, Republic of Korea
[b] Department of Civil and Environmental Engineering, Korea Advanced Institute of Science and Technology (KAIST), 291 Daehak-ro, Yuseong-gu, Daejeon 34141, Republic of Korea
[c] Institute of Advanced Composite Materials, Korea Institute of Science and Technology (KIST), 92 Chudong-ro, Bongdong-eup, Wanju-gun, Jeonbuk 55324, Republic of Korea
[d] School of Civil Engineering, Chungbuk National University, 1 Chungdae-ro, Seowon-gu, Cheongju, Chungbuk 28644, Republic of Korea

ARTICLE INFO

Keywords:
A. Swarm intelligence
B. Micromechanics
C. Thermal conductivity
D. Thermoplastic composites

ABSTRACT

With the recent demand for miniaturization and integration of electronic devices, there has been a growing interest in device malfunction due to high temperature. In this study, a experimental and theoretical study on the composites with improved thermal conductivity by dispersing multi-walled carbon nanotubes (MWCNTs) in the thermoplastic resin was carried out. A micromechanical model was derived based on the ensemble volume-averaging method and the modified Eshelby's tensor reflecting the interface properties. The effects of the waviness, interface, and orientation of fillers on the thermal conductivity of composites were numerically analyzed. A computational intelligence-based particle swarm optimization (PSO) algorithm was adopted to the proposed model for optimizing the model constants. The thermal conductivity of the polymerized cyclic butylene terephthalate (pCBT)/MWCNT composites was experimentally measured according to the content of MWCNT. Finally, the experimentally measured data were utilized in the PSO to improve the predictive capability of the proposed model.

1. Introduction

There is a growing demand for electronic devices with various functions and portability, and with these trends, electronic devices are becoming increasingly integrated and miniaturized [1]. Such changes in electronic devices increase potential risks such as failure, malfunction, and fire caused by heat emitted from electronic devices, and there is a growing interest in the control of emitted heat [2]. In this context, there is a need for a thermal management material that is lightweight, has excellent thermal conductivity, and exhibits good processability that can be easily applied in a small space [3]. As a result, there is a growing interest in high thermal conductivity polymer composites comprising metal and ceramic fillers having excellent thermal conductivity and a polymer matrix having low thermal conductivity but excellent processability [4].

Since various experimental methods have been developed to improve the performance of high thermal conductivity polymer composites, there is a growing demand for a modeling technique capable of precisely predicting the thermal conductivity of the composite material in consideration of these various environments and conditions. A model for predicting thermal conductivity of nanocomposites has recently been proposed by various researchers as micromechanics-based theory. Yin et al. [5,6] proposed a self-consistent model to analyze the effective thermal conductivity and heat flux field of particle-embedded nanocomposites. The Kapitza thermal resistance between the particle and matrix is considered theoretically, and the validity of the model [5,6] was verified through various methods. Chen et al. [7] and Su et al. [8] proposed a thermal conductivity prediction model that takes into account the interfacial region between the filler and the matrix.

In addition, Lee et al. [9] proposed a modified Eshelby's tensor considering interface effect. They applied the newly proposed Eshelby's tensor to Mori-Tanaka method, and theoretically analyzed the interface effects on the thermal conductivity of composites [9]. However, it is very difficult to measure the exact value of the interface experimentally and therefore has relied on the fitting of experimental results. To overcome these limitations, recently, Kim et al. [4] proposed a

* Corresponding author.
E-mail address: byang@chungbuk.ac.kr (B. Yang).

https://doi.org/10.1016/j.compositesa.2019.105646
Received 8 July 2019; Received in revised form 30 August 2019; Accepted 22 September 2019
Available online 24 September 2019
1359-835X/

multiscale analysis method combining molecular dynamics (MD) simulation and micromechanics. Such a multiscale method is theoretically close to reality; however, it has a disadvantage in that it takes considerably long time and computation expense to analyze complex materials. In addition, there is a difficulty in constructing different composite systems each time for a new matrix-inclusion combination.

With the recent demand for reliable and facile model for functional composites, we developed a computational intelligence (CI) integrated micromechanical model based on Eshelby's equivalent inclusion principle of the effective medium approach and the ensemble volume averaging method was proposed in this study. For a more realistic prediction, the waviness and interface properties of the MWCNT were considered in the micromechanical model. A series of numerical studies was carried out to investigate the effect of model parameters, and a CI-based particle swarm optimization (PSO) algorithm was applied to the derived micromechanical model to optimize the model constants. In addition, the thermal conductivity of the polymerized cyclic butylene terephthalate (pCBT)/MWCNT composites was experimentally measured according to the content of MWCNT, and the material properties were evaluated by field emission scanning electron microscopy (FE-SEM), micro-computed tomography (micro-CT), wide angle X-ray diffraction (WAXD), and differential scanning calorimetry DSC analyses. The predictions were compared with the present experimental results to verify the validity of the proposed model.

2. Micromechanical modeling of the composites

2.1. The effective thermal conductivity of the composites considering with waviness and interface effects

By utilizing Eshelby's equivalent inclusion principle of the effective medium approach and Ju and Chen's ensemble volume averaging method, initially developed for elastic properties estimation of composite materials, the thermal conductivity of a composite material with a three dimensional random orientation of inclusions can be determined as follows [10–12]

$$\mathbf{K}^{*} = \mathbf{K}_0 \cdot [\mathbf{I} + \mathbf{B} \cdot (\mathbf{I} - \mathbf{S} \cdot \mathbf{B})^{-1}] \tag{1}$$

$$\mathbf{B} = \phi_1 (\mathbf{S} + \mathbf{A}_1) \tag{2}$$

$$\mathbf{A}_1 = (\mathbf{K}_1 - \mathbf{K}_0)^{-1} \cdot \mathbf{K}_0 \tag{3}$$

where $\mathbf{K}^{*}$, $\mathbf{S}$, ϕ_1 are the effective thermal conductivity tensor of composites, the Eshelby's tensor, volume fraction of inclusions. $\mathbf{K}_0$ and $\mathbf{K}_1$ denote the thermal conductivity tensor of the matrix and inclusion, respectively [8–10]. The nano-sized inclusion (filler) was assumed to be uniformly dispersed and 3D randomly oriented in the matrix. For steady state heat conduction problems, the Eshelby's tensor $\mathbf{S}$ is analogous to the fourth order Eshelby's tensor (S_{ijkl}) for elasticity problems, but becomes a second order tensor S_{ij} for the prediction of thermal conductivity [13,14]. For inclusions in an isotropic matrix, the Eshelby's tensor mainly depends on the shape and aspect ratio of inclusions. The Eshelby's tensor for spheroidal inclusion in an isotropic medium is given by [14]

$$S_{11} = S_{22} = \frac{a_2^2 a_3}{2(a_3^2 - a_2^2)^{3/2}} \left[\frac{a_3}{a_2} \left(\frac{a_3^2}{a_2^2} - 1 \right)^{1/2} - \cosh^{-1} \frac{a_3}{a_2} \right] \tag{4}$$

$$S_{33} = 1 - S_{22} \tag{5}$$

Here, for prolate spheroidal ($a_1 = a_2 < a_3$), a_3 denotes the length of longer direction (See, Fig. 1(a)).

During the manufacturing process, the inclusions tend to be distorted and lose their original shapes. This distortion is referred to as waviness of the inclusion, and can be addressed by considering the change in the original length and width of the inclusions. As shown in Fig. 1(b), the degree of waviness would depend on the angle θ_w that determines the amplitude and period of the cosine function, representing the change in length and width of the inclusion [15,16]. The cosine function for describing the waviness is given by [16]

$$\mathrm{y} = \cos(\tan\theta_w \cdot x) \tag{6}$$

Herein, Eq. (6) is a mathematical expression of the MWCNTs morphology that is wave-shaped in a cosine with a range of one period. x and y signify the length and height of the MWCNT with respect to θ_w. When the MWCNT is fully extended, x is equal to the initial length of the filler and y is zero. Note that Eq. (6) is valid assuming that x increases and y decreases at the same ratio as θ_w increases regardless of the initial length of MWCNT. A schematic explanation of the MWCNT waviness is detailed in Fig. 6 of [16]. The length of the cosine graph $f(\theta_w)$ from $(0 \le \mathrm{x} < \frac{2\pi}{\tan\theta_w})$,which should be the same as the length of the inclusion ($f(\theta_w) = a_3$), where $2\pi/\tan\theta_w$is the new period of the cosine function graph. Therefore, it is given by [16]

$$f(\theta_w) = \int_0^{\frac{2\pi}{\tan\theta_w}} \sqrt{\mathrm{d}x^2 + \mathrm{d}y^2} = \int_0^{\frac{2\pi}{\tan\theta_w}} \sqrt{1 + [\tan\theta_w \{-\sin(x \cdot tan\theta_w)\}]^2}\, \mathrm{d}x \tag{7}$$

By scaling the amplitude and the period of cosine function, the new cosine function becomes [16]

$$\mathrm{y} = \frac{a_3}{f(\theta_w)} \cos\left[\tan(\theta_w) \hat{\mathrm{A}} \cdot \frac{x f(\theta_w)}{a_3} \right] \tag{8}$$

From the above relations the new length and width of the inclusion becomes [16]

$$a_3^{'} = \frac{2\pi}{\tan\theta_w} \hat{\mathrm{A}} \cdot \frac{a_3}{f(\theta_w)}, \quad a_1^{'} = a_2^{'} = a_2 + \frac{2a_3}{f(\theta_w)} \tag{9}$$

In addition, due to the existence of a thermal resistance at the interface between the inclusion and matrix, a jump in the temperature field is observed while the heat flux remains constant [9]. When the interface thermal resistivity is considered the temperature fields inside and outside the inclusion are defined as follows [17]:

$$T^{out} - T^{in} = -\alpha \cdot q \cdot n \tag{10}$$

where α is the Kapitaz thermal resistance at interfacial region that causes the disturbance in the temperature field (See, Fig. 1(c)). q and n are the heat flux and the outward normal vector of the inclusion. For thermal conductivity problems, similar to elasticity problems, Eshelby's tensor relates the intensity field or the temperature gradient with the eigen-intensity field [14], and can be modified considering interface characteristics as $\mathbf{S}^{M}$ [9]. By replacing $\mathbf{S}$ in Eqs. (1) and (2) with $\mathbf{S}^{M}$ in [9], the effects of Kapitza thermal resistance between the inclusion and matrix can be reflected in the present model. All theoretical concepts and derivation processes of $\mathbf{S}^{M}$ are described in detail and clarity in [9].

2.2. Random orientation of inclusion

As the geometrical arrangement of the inclusions inside the matrix significantly affects the thermal conductivity of the composites, representing the three-dimensional random orientation of the inclusions, we adopted an orientational averaging process given by [9,16,17]

$$\langle \mathbf{A} \rangle = \frac{\int_{-\pi}^{\pi} \int_0^{\pi} \int_0^{\pi} W(\tau) \mathbf{R} \cdot \mathbf{A} \cdot \mathbf{R}^{\mathrm{T}} sin\gamma \mathrm{d}\tau \mathrm{d}\gamma \mathrm{d}\varphi}{\int_{-\pi}^{\pi} \int_0^{2\pi} \int_0^{\pi} \sin\gamma \mathrm{d}\tau \mathrm{d}\gamma \mathrm{d}\varphi} = \frac{1}{4\pi^2} \int_{-\pi}^{\pi} \int_0^{\pi} \int_0^{\pi} W(\tau) \mathbf{R} \cdot \mathbf{A} \cdot \mathbf{R}^{\mathrm{T}} \sin\gamma \mathrm{d}\tau \mathrm{d}\gamma \mathrm{d}\varphi \tag{11}$$

with the 3D transformation tensor $\mathbf{R}$ expressed as follows [18]

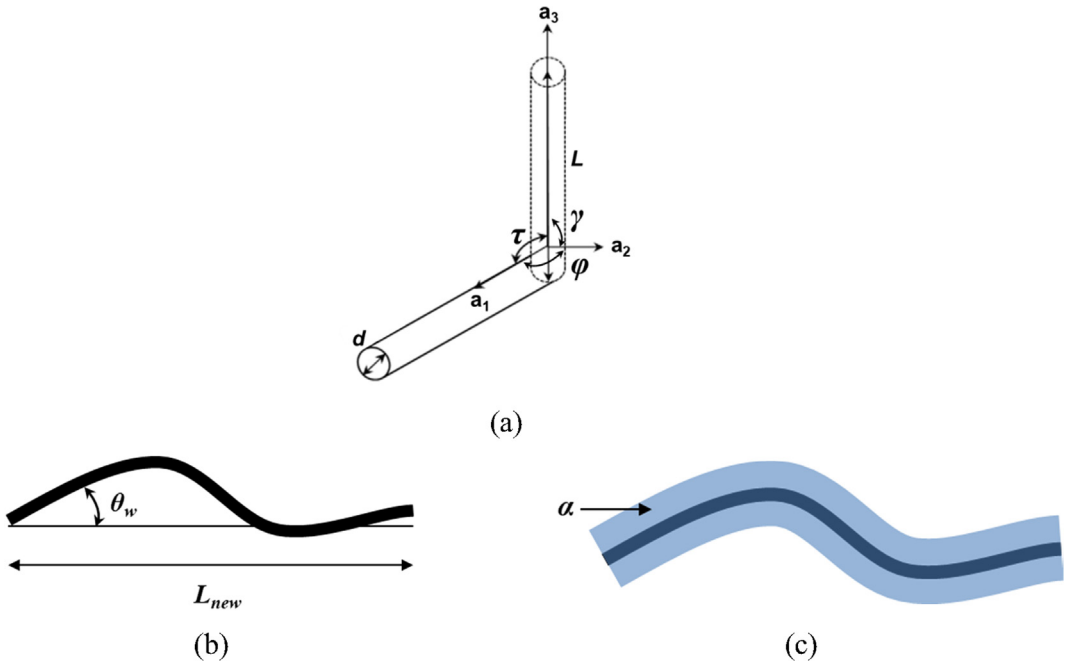

Fig. 1. (a) Theoretical axis of inclusions considered in the present study and schematic representations of (b) degree of waviness (θ_w) and (c) interface (α) characteristics. (For interpretation of the references to colour in this figure legend, the reader is referred to the web version of this article.)

$$R = \begin{bmatrix} \cos(\tau)\cos(\varphi) - \sin(\tau)\cos(\gamma)\sin(\varphi) & \sin(\tau)\cos(\varphi) + \sin(\tau)\cos(\gamma)\sin(\varphi) & \sin(\varphi)\sin(\gamma) \\ -\cos(\tau)\sin(\varphi) - \sin(\tau)\cos(\varphi)\cos(\gamma)\cos(\varphi) & -\sin(\tau)\sin(\varphi) + \cos(\varphi)\cos(\gamma)\cos(\varphi) & \sin(\gamma)\sin(\varphi) \\ \sin(\varphi)\sin(\gamma) & -\cos(\tau)\sin(\gamma) & \cos(\gamma) \end{bmatrix} \tag{12}$$

where $W(\tau)$ is the random orientation distribution function (ODF), defining the degree to which the inclusions are randomly oriented in the matrix [19–21]. The ODF is given by

$$W(\tau) = \frac{\sigma\cosh(\sigma cos(\tau))}{\sinh(\sigma)} \tag{13}$$

where σ is the parameter accounting for the degree of the preferred alignment. In the special case of $\sigma = 0$ that is meaning no degree of preferred orientation, $W(\tau) = 1$. Hence after applying the random orientation, the effective thermal conductivity of the nanocomposite becomes

$$\ll \mathbf{K}_{eff} \gg = \mathbf{K}_0 \cdot [\mathbf{I} + \ll \mathbf{B} \gg \cdot (\mathbf{I} - \mathbf{S}^M \cdot \mathbf{B})^{-1}] \tag{14}$$

2.3. The PSO algorithm

The PSO is the global optimization algorithms utilized in the field of computer science [22]. Through iterative calculations, the candidate solutions are simultaneously improved, and finally the objective function optimization is achieved [23]. In this study, the PSO algorithm illustrated in Fig. 2 and Table 1 was adopted to estimate the model parameters (θ_w and α). In order for the PSO to be integrated to the proposed model, the following processes were performed (Fig. 2) [22]:

(1) Input the material constants: These values such as the thermal conductivities of the matrix and MWCNT, and length/diameter of MWCNT were obtained from the experiment. (2) Select the model constants: In this study, θ_w and α were selected as the unknown parameter to be found through PSO. (3) Apply the error variation: The model constants were completely determined by the experimental results; however, all experiments involve a certain level of human-induced error. Herein, it was assumed that there is an error of 0.1% and 1% in the content and length of MWCNT conducted in the experiment, respectively. Although it raises the uncertainty of the analysis, it can provide closer conditions to the actual experiment. (4) Calculation: When the new calculation is closer to the experiments than the previous calculation, the result is updated with the new values. Otherwise, the new prediction is discarded, and the existing prediction remains. The parameters are updated by the following equations: $x_{id} = x_{id} + v_{id}$; $v_{id} = w \cdot v_{id} + c_1 \cdot r_1(p_{id} - x_{id}) + c_2 \cdot r_2(p_{gd} - x_{id})$, where $\times$, v, c, and p denote the position and velocity of particle; self and social acceleration coefficients; personal and neighborhood bests, respectively. A more detailed description of the meaning of each constant is given in the references [23]. (6) It is repeated for the number of populations specified, so as to derive the most optimized model constants that can reflect the most accurate prediction results. The aforementioned descriptions of PSO process are summarized in Table 1.

3. Experimental program

3.1. Materials

MWCNT (Jenotube 8, JEIO Co., Inchon, Korea) was used as a filler to improve the thermal conductivity of the composite films. The filler used was a one-dimensional carbon allotrope with length and diameter of 100–200 μm and 7–9 nm, respectively. Cyclic butylene terephthalate (CBT, CBT 160, Cyclics® Co., Schenectady, NY, USA) was used as the matrix of the composite films. CBT is a low molecular weight cyclic oligomer composed of 2 to 7 butyl monomers. CBT exhibited melt and flow characteristics at 130–150 °C. When heated above 160 °C, it was polymerized by the contained catalyst to become pCBT [24–27] In addition, the manufacturing process of the present composites through in-situ polymerization resin with highly dispersed MWCNT filler is addressed in Fig. 3.

3.2. Fabrication

Residual moisture can interfere with the polymerization reaction of the CBT resin, hence, the filler and the resin were dried at 100 °C for

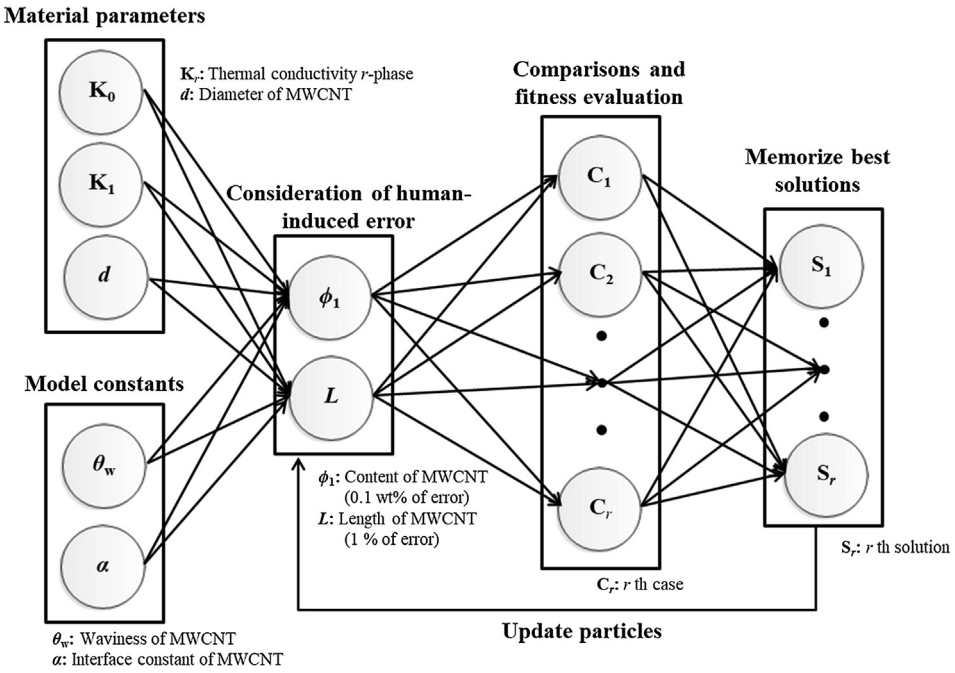

Fig. 2. Schematic diagram of the present PSO process.

Table 1
The calculation process of PSO in the present study [23].

Step 1: Input the material constants and initialize a population of particles.
Step 2: Select the model constants (θ_w and α) and determine the error variations (ϕ_1 and l).
Step 3: Evaluate the adequate population with the following equation: $x_{id} = x_{id} + v_{id}$; $v_{id} = w \cdot v_{id} + c_1 \cdot r_1(p_{id} - x_{id}) + c_2 \cdot r_2(p_{gd} - x_{id})$ where the definitions of each constant are described in the manuscript.
Step 4: Run the main searching process until population index reaches the population size: Update the personal best, neighborhood best, velocity, and position.
Step 5: Check the population index and global closeness.
Step 6: Generate the next population and update the internal weight until the general index reaches the maximum generation.
Step 7: Check the general index is equal to the maximum generation or the prediction is sufficiently good fitness. Terminate the PSO when either of the two conditions is met.

12 h to remove moisture before composite fabrication. Since the viscosity of the CBT at the initial melting was as low as 0.02 Pa·s, the dispersion of the incorporated filler and the interface between the filler and the resin can be excellently induced. To induce good dispersion, the CBT pellets were made into fine powder as shown in Fig. 3, blended with the filler at a target weight ratio, and then mixed with a mixing machine (ARE 310, Thinky Corp., Tokyo, Japan) at 2000 rpm for 3 min. The mixed powder was heated using a hot press at 230 °C for 20 min. CBT was in-situ polymerized, and then composite films were produced at 300 psi for 1 min continuously. Previous studies have reported that polymer composites filled with uniformly incorporated carbon fillers can be prepared using the low viscosity of the reactive polymeric resin. In addition, composites in which fillers are uniformly dispersed are essential for validating the proposed modeling.

3.3. Characterization

3.3.1. Crystalline structure

WAXD measurements were performed using an X-ray diffractometer (PANalytical X'Pert Pro, Malvern Panalytical Ltd., Royston, UK) equipped with a Giono-meter PW3050/60 working with Cu K alpha radiations (1.540598 Å) to analyze the crystalline structure of the fabricated composites. Intensity of the diffraction was recorded by continuous scanning at a rate of 0.02 deg/s over a range of $10 < 2\theta < 60$ deg (θ = Bragg angle).

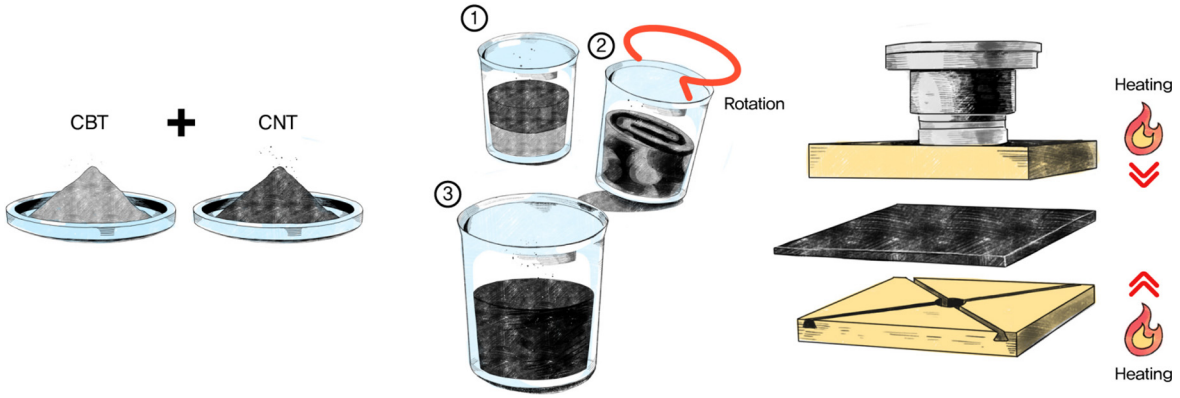

Fig. 3. Schematics of manufacturing process of one-step composite film through in-situ polymerization resin with highly dispersed MWCNT filler. (For interpretation of the references to colour in this figure legend, the reader is referred to the web version of this article.)

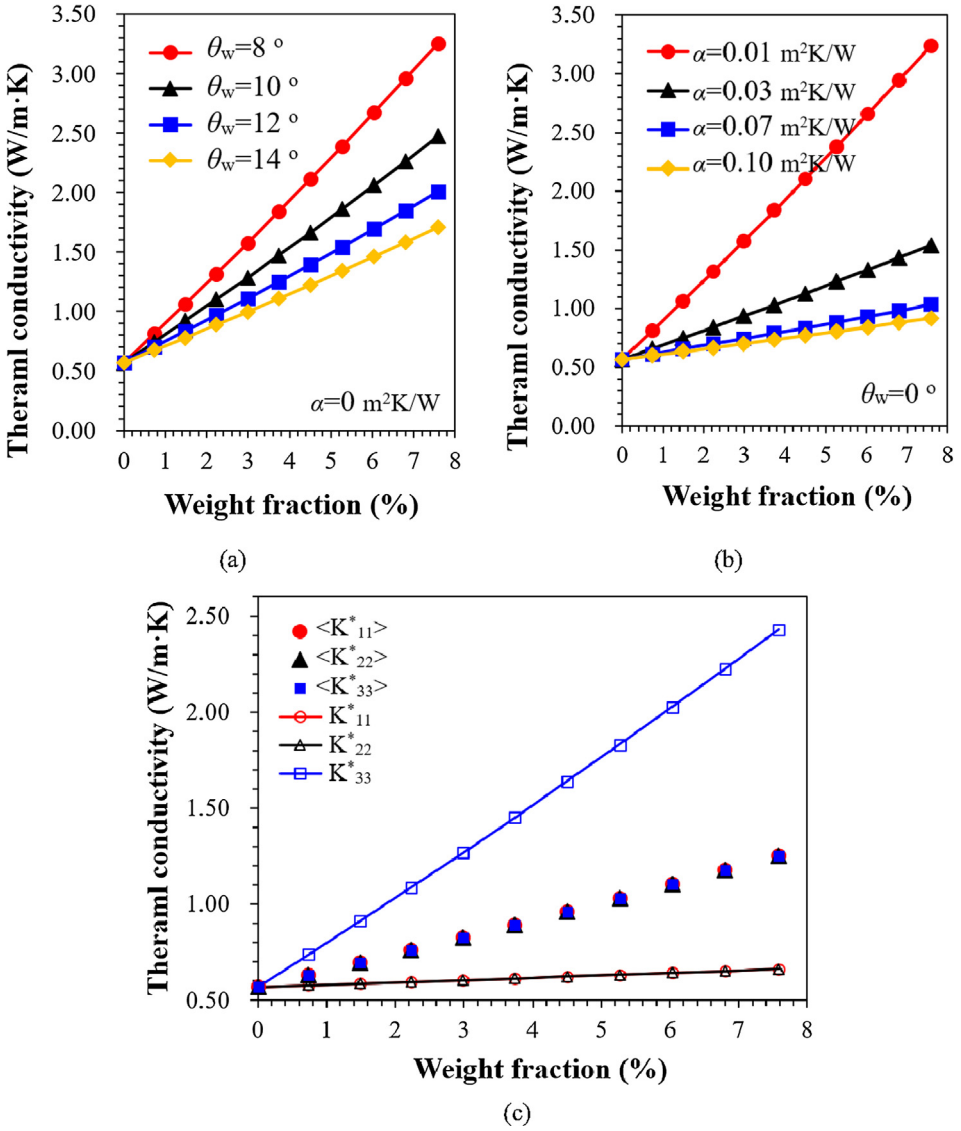

Fig. 4. Numerical analyses to investigate effects of (a) θ_w, (b) α, and (c) filler orientation on the effective thermal conductivity of nanocomposite. (For interpretation of the references to colour in this figure legend, the reader is referred to the web version of this article.)

3.3.2. Thermal behavior

The crystallization and melting temperature of the CBT, pCBT and composites were measured using DSC (Q20, TA Instrument, DE, USA) with a nitrogen atmosphere in the temperature range of 50–250 °C. The composites were heated from 50 to 250 °C at a rate of 10 °C/min and maintained at 250 °C for 5 min. After that, the specimens were cooled to 50 °C at a rate of 10 °C/min. Measurements were performed by repeating the procedure twice.

3.3.3. Morphology

The diameter and length of the MWCNT filler and the fracture surface of the composite films were observed using a field emission scanning electron microscope (FE-SEM, Nova NanoSEM 450, FEI Corp., OR, USA). The prepared samples were coated with platinum under vacuum using a sputtering coating machine (Ion Sputter E-1030, Hitachi High Technologies, Tokyo, Japan) for 110 sec. The coated composite specimens were observed under a nitrogen vacuum at a current of 10 kV. Micro-computed tomography (Micro-CT, Skyscan 1172, Bruker Co., Billerica, MA, USA) with resolution of 700 nm was used to observe the three-dimensional (3D) MWCNT aggregates of the fabricated composite films.

3.3.4. Thermal conductivity

The thermal conductivity of composite films was measured in accordance with ISO 22007-2 using thermal conductivity measurement equipment at room temperature and normal pressure. The sensor used consisted of a double helix of thin nickel wire and was operated as the heat source of the continuous plate. As the sensor was supplied with constant power (P), temperature rise (ΔT) and resistance change were induced. This change was used to measure the temperature change of the sensor itself. The thermal conductivity of the specimen was determined by calculating the solution of the Fourier equation for the thermal conductivity based on the supplied power and the induced temperature change.

4. Results and discussion

A series of numerical simulations are carried out to investigate the influences of the waviness and interface properties of inclusions on the effective thermal conductivity of composites ($\mathbf{K}^*$). We adopted the material constants of MWCNT-reinforced CBT matrix composite in accordance with measurements as: $K_0 = 0.57\ Wm^{-1}K^{-1}$, $K_1 = 1950\ Wm^{-1}K^{-1}$, $l = 150\ \mu m$, $d = 8.5\ nm$, $\rho_{CBT} = 1440\ kg/m^3$ and $\rho_{MWCNT} = 2200\ kg/m^3$. The set of model parameters were

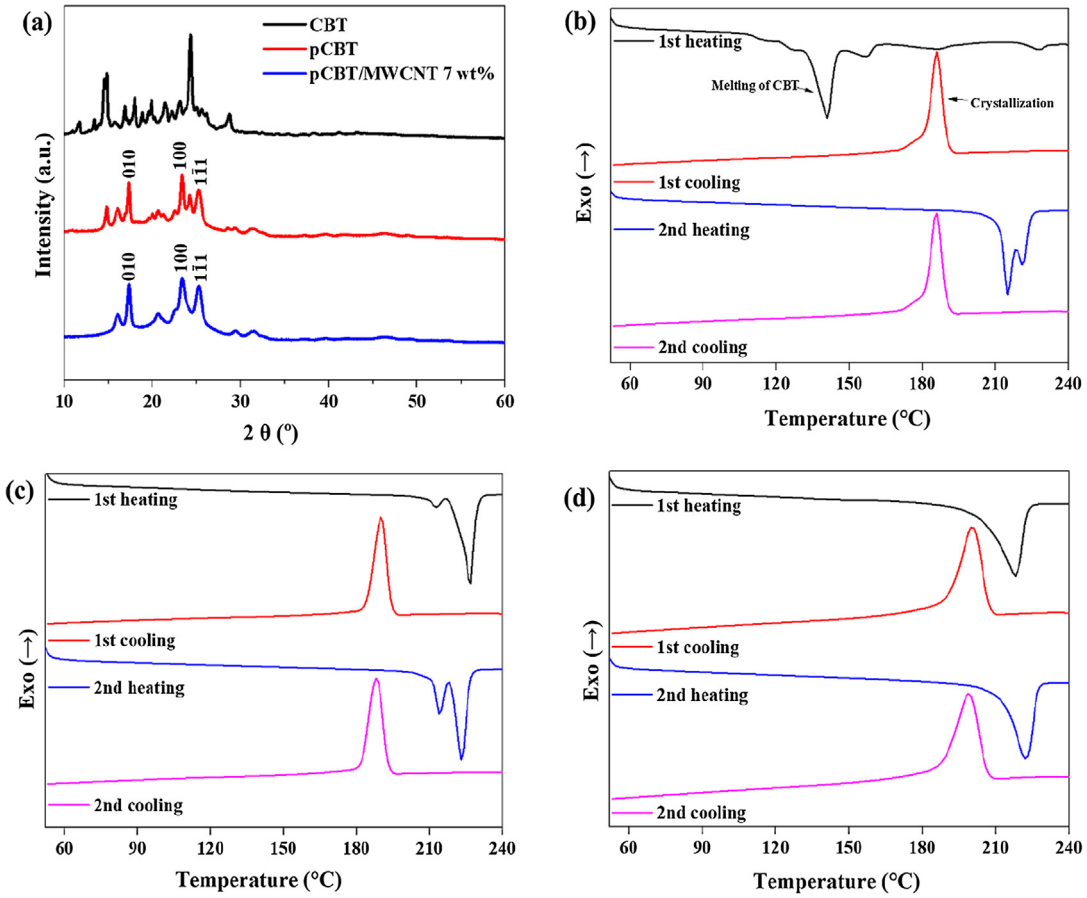

Fig. 5. (a) WAXD profiles of the CBT, pCBT and composite fabricated using proposed process and DSC thermograms of the (b) CBT, (c) pCBT and (d) composite fabricated using the proposed process. (For interpretation of the references to colour in this figure legend, the reader is referred to the web version of this article.)

considered as: θ_w = 8, 10, 12, and 14° with α = 0 m^2K/W; α = 0.01, 0.03, 0.07, and 0.10 m^2K/W with θ_w = 0°. It is shown from Fig. 4(a) that the thermal conductivity becomes higher as θ_w continues to decrease. Reduced θ_w means that the MWCNT inclusion is ideally straight, which could have a positive impact on the effective thermal conductivity. Otherwise, as the value of α increases, the predicted effective thermal conductivity decreases. This implies that the effect of the Kapitza interface disappears as α goes to zero (Fig. 4(b)). The interfacial effect gradually decreases as the α increases, ultimately diminishing when the α reaches 0.10 m^2K/W [28].

Additional numerical analysis was performed to investigate the effect of the filler orientation on the thermal conductivity of composites. The effective thermal conductivity with different filler orientations is shown in Fig. 4(c). Herein, we consider the case where the MWCNTs are uniformly aligned in each axial direction (11, 22, and 33), and the 3D randomly distributed. Through this, the thermal conductivity of the composites was predicted according to the filler orientation. A fairly high thermal conductivity value is predicted when MWCNT is perfectly aligned in the filler direction (33); however, a low value is predicted for the other two directions. In case of random orientation, intermediate values are predicted for the two preceding values and have the same thermal conductivity values for all directions. Since it is impossible to arrange the nano-sized fillers in the thermoplastic matrix in a single direction, considering the randomness of filler orientation would be a more realistic prediction. Through the proposed model, the influence of the filler orientation on the effective thermal conductivity of the composites could be analytically evaluated.

WAXD patterns of the composites were analyzed to determine in-situ polymerization of CBT in the proposed process as shown in Fig. 5(a). The crystalline peaks of CBT powder indicate that the CBT resin is composed of 2–7 crystalline oligoesters. The difference between the WAXD patterns of CBT and pCBT was due to the crystallization occurring when CBT oligomer was in-situ polymerized to pCBT polymer [29,30]. As shown in Fig. 5(b), the thermal behaviors of the CBT and the fabricated composites were analyzed using DSC. During the first heating, the first melting peak of the CBT resin was observed in the range of 130–150 °C [30,31]. Furthermore, the endothermic peak observed in the range of 220–235 °C was due to melting of the pCBT [30,31]. The exothermic peak near 186 °C observed during the first cooling of the CBT resin was determined as the peak due to the crystallization of the molten pCBT [30]. Unlike the first heating, no endothermic peak was observed in the range of 130–150 °C in the second heating. This result indicated that in-situ polymerization of CBT oligomer was completed during DSC scans [30,31].

The DSC curves of pCBT (Fig. 5(c)) were similar to the second cycle of CBT. The melting (220–235 °C) and crystallization (near 186 °C) peaks were observed respectively in the second heating and cooling of the polymerized CBT during the first heating occurred in the same range as the peaks of pCBT [30]. No melting peak of CBT was observed during the first heating of the fabricated composite (Fig. 5(d)). This indicated that the CBT resin was polymerized to the pCBT polymer in the proposed process. The endothermic peaks occurring during the first and second heating were due to the melting of the polymer, like the peaks of pCBT. However, the crystallization peak was observed at around 200 °C. It was attributed to the fact that MWCNT acts as a nucleating agent [32]. As a result, it was confirmed by the results of WAXD and DSC that the CBT oligomers inside the composite material were well polymerized to pCBT polymers.

The FE-SEM images of the bundle length and single strand thickness of the MWCNT used and the fracture surface of the pCBT/MWCNT

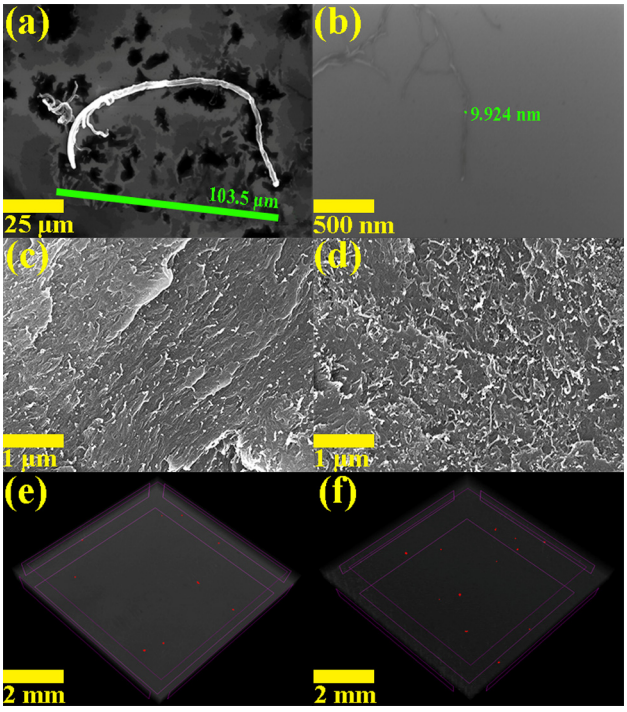

Fig. 6. (a) Bundle length and (b) single strand diameter of MWCNT used in composite fabrication, and FE-SEM images of fracture surfaces of the fabricated composite films filled with MWCNT of (c) 3 wt% and (d) 7 wt%, and micro-CT images of the fabricated composite films filled with MWCNT of (e) 3 wt% and (f) 7 wt%. (For interpretation of the references to colour in this figure legend, the reader is referred to the web version of this article.)

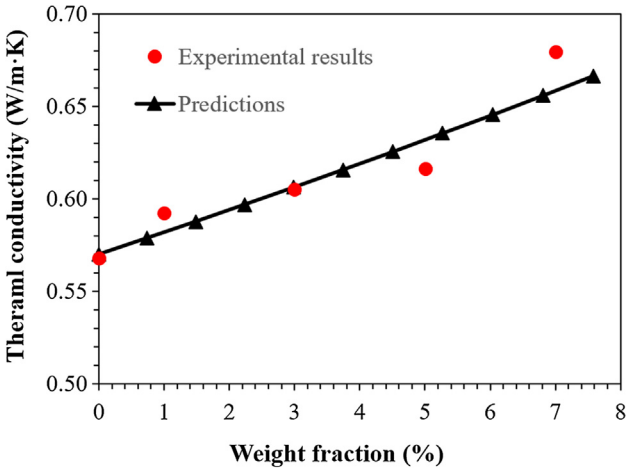

Fig. 7. Comparisons between experimental measurements and micro-mechanics-based predictions. (For interpretation of the references to colour in this figure legend, the reader is referred to the web version of this article.)

composite film produced by the proposed process according to the filler weight fraction were shown in Fig. 6(a–d). Through the observation of the fracture surface, an attempt was made to evaluate the distribution level of the MWCNT filler. Excellent dispersion was observed at the fracture surface of the composite containing 7 wt% or less filler. Micro-CT analysis was performed to observe MWCNT dispersion and filler aggregates of 700 nm size or larger inside the fabricated composites. Unlike two-dimensional FE-SEM analysis, Micro-CT can analyze non-destructively a relatively large area (~50 mm^3) of a specimen in three dimensions. As shown in Fig. 6(e) and 6(f), the MWCNT aggregates were rarely observed in the composite fabricated by the proposed process. Therefore, it was confirmed that the proposed manufacturing method is a low-cost one-step process (no solvent) capable of uniformly dispersing the MWCNT filler [24,33].

The thermal conductivity of the manufactured composite film is shown in Fig. 7. As the content of MWCNT increased, the thermal conductivity of composite films was increased. The thermal conductivity of the composite films incorporating 7 wt% MWCNT was 0.68 W/m·k, which was 20% higher than the resin used. The low thermal conductivity of the fabricated composites was due to the interface resistance between the MWCNT and the polymer resin. Predictions based on the micromechanical model were compared with experimental data to evaluate the effectiveness of the experimental study. In the present study, ten specimens were prepared according to the MWCNT content, and the mean values of the experimental results were compared with the predictions. The experimentally measured thermal conductivity of 3D randomly oriented MWCNT-embedded nanocomposite was utilized, and the comparisons are made with the fixed model constants: $\theta_w = 10^\circ$ and $\alpha = 0.8\ m^2K/W$. The aforementioned model constants were derived via the PSO calculation. Fig. 7 shows that the overall thermal conductivity of nanocomposites with MWCNT, and good agreements between predictions and experimental results is observed.

For further verification, the predictions based on the proposed model were compared with other experimental data in literatures [34,35]. First, the present predictions on single-walled carbon nanotube (SWNT)-embedded polyethylene nanocomposites were compared with the experimental data [34]. The same material properties as reported in [34] were utilized as: $K_0 = 0.5\ Wm^{-1}K^{-1}$, $K_1 = 3000\ Wm^{-1}K^{-1}$, $l = 445$ nm, $d = 3$ nm. The derived model parameters through PSO were: $\theta_w = 10^\circ$ and $\alpha = 0.01\ m^2K/W$. In addition, predictions on epoxy nanocomposites with two different types of MWCNTs (pristine and surface functionalized) were made with the same material properties as reported in [35]: $K_0 = 0.3\ Wm^{-1}K^{-1}$, $l = 10\ \mu m$, $d = 80$ nm. Since thermal conductivity of MWCNT was not given in [35], it was assumed to be the same value as applied in this study, $K_1 = 1950\ Wm^{-1}K^{-1}$. The model constants for pristine MWCNT-reinforced epoxy matrix were estimated as: $\theta_w = 5^\circ$ and $\alpha = 0.055\ m^2K/W$, while the case of composites with surface functionalized MWCNT is: $\theta_w = 5^\circ$ and $\alpha = 0.025\ m^2K/W$. Fig. 8 shows another good agreement between the experimental data [34,35] and the present predictions.

5. Conclusions

In the present study, the theoretical and experimental study on the composites with improved thermal conductivity by dispersing MWCNTs in the thermoplastic resin was carried out. In particular, the effect of interface, waviness, and orientation of the spheroidal MWCNT inclusions in the composites on the effective thermal characteristics was theoretically predicted. The main features of the present study are to propose a model that can comprehensively consider the waviness and interface effects of inclusions, to propose a specific algorithm to optimize the model constant, and to consider the human-induced error that may occur in the manufacturing process of composites.

The proposed micromechanical model was based on the micromechanical ensemble volume averaging method and modified Eshelby's tensor reflecting the interface properties. Experimentally, the thermal conductivity of the pCBT/MWCNT composites was measured according to the content of MWCNT, and the dispersibility of the filler was evaluated by SEM and micro-CT analyses. XRD and DSC analyzes were also performed to verify the validity of the experimental data. The results of the measurements were compared with the PSO integrated micromechanical model. It was confirmed that the measured results of thermal conductivity of the composites with MWCNT filler are in agreement with the theoretical predictions.

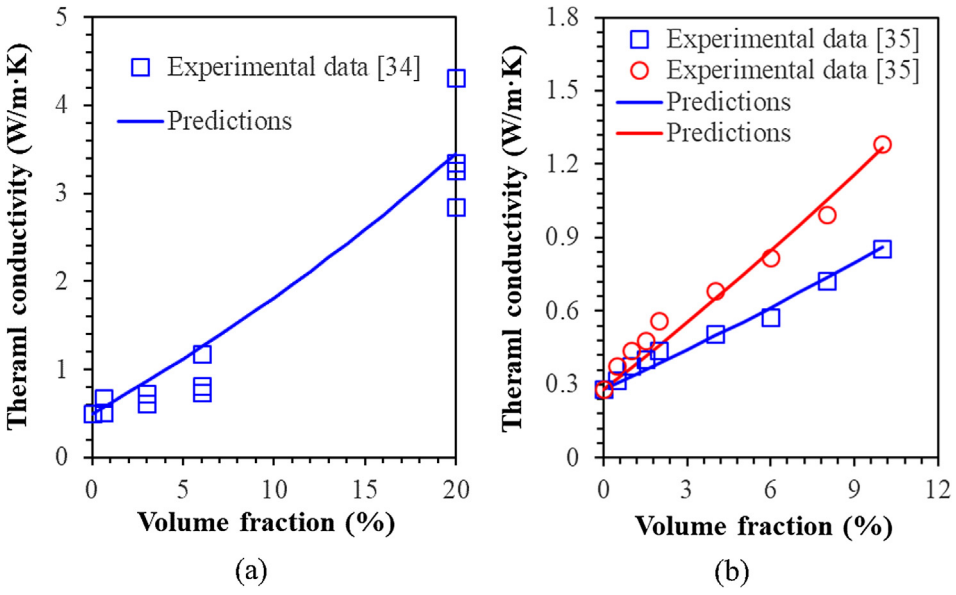

Fig. 8. The comparisons of thermal conductivities of (a) single-walled carbon nanotube/polyethylene nanocomposites and (b) epoxy composites containing pristine MWCNT and surface functionalized MWCNT. (For interpretation of the references to colour in this figure legend, the reader is referred to the web version of this article.)

Declaration of Competing Interest

The authors declare that they have no known competing financial interests or personal relationships that could have appeared to influence the work reported in this paper.

Acknowledgments

This work was supported by the research grant of the Chungbuk National University in 2018, Basic Science Research Program (2017R1C1B5077037) through the National Research Foundation of Korea (NRF) funded by the Ministry of Education, and the Industrial Technology Innovation Program (10082586) funded by the Ministry of Trade, Industry & Energy of Korea.

References

[1] Mohammed MI, Haswell S, Gibson I. Lab-on-a-chip or Chip-in-a-lab: challenges of commercialization lost in translation. Procedia Technol 2015;20:54–9.
[2] Fok S, Shen W, Tan F. Cooling of portable hand-held electronic devices using phase change materials in finned heat sinks. Int J Therm Sci 2010;49(1):109–17.
[3] Li X-H, Li X, Liao K-N, Min P, Liu T, Dasari A, et al. Thermally annealed anisotropic graphene aerogels and their electrically conductive epoxy composites with excellent electromagnetic interference shielding efficiencies. ACS Appl Mater Interfaces 2016;8(48):33230–9.
[4] Kim SY, Jang HG, Yang C-M, Yang B. Multiscale prediction of thermal conductivity for nanocomposites containing crumpled carbon nanofillers with interfacial characteristics. Compos Sci Technol 2018;155:169–76.
[5] Yin H, Paulino G, Buttlar WG, Sun L. Effective thermal conductivity of functionally graded particulate nanocomposites with interfacial thermal resistance. J Appl Mech 2008;75(5):051113.
[6] Yin H, Paulino G, Buttlar WG, Sun L. Heat flux field for one spherical inhomogeneity embedded in a functionally graded material matrix. Int J Heat Mass Transf 2008;51(11–12):3018–24.
[7] Chen T, Weng GJ, Liu W-C. Effect of Kapitza contact and consideration of tube-end transport on the effective conductivity in nanotube-based composites. J Appl Phys 2005;97(10):104312.
[8] Su Y, Li JJ, Weng GJ. Theory of thermal conductivity of graphene-polymer nanocomposites with interfacial Kapitza resistance and graphene-graphene contact resistance. Carbon 2018;137:222–33.
[9] Lee S, Lee J, Ryu B, Ryu S. A micromechanics-based analytical solution for the effective thermal conductivity of composites with orthotropic matrices and interfacial thermal resistance. Sci Rep 2018;8(1):7266.
[10] Ju J, Chen T. Micromechanics and effective moduli of elastic composites containing randomly dispersed ellipsoidal inhomogeneities. Acta Mech 1994;103(1–4):103–21.
[11] Nemat-Nasser S, Hori M. Micromechanics: overall properties of heterogeneous materials. Elsevier; 2013.
[12] Yang B, Souri H, Kim S, Ryu S, Lee H. An analytical model to predict curvature effects of the carbon nanotube on the overall behavior of nanocomposites. J Appl Phys 2014;116(3):033511.
[13] Eshelby JD. The determination of the elastic field of an ellipsoidal inclusion, and related problems. Proc R Soc Lond Ser A Math Phys Sci 1957;241(1226):376–96.
[14] Hiroshi H, Minoru T. Equivalent inclusion method for steady state heat conduction in composites. Int J Eng Sci 1986;24(7):1159–72.
[15] Stewart J. Multivariable calculus: Nelson Education; 2015.
[16] Kim G, Yang B, Cho K, Kim E, Lee H. Influences of CNT dispersion and pore characteristics on the electrical performance of cementitious composites. Compos Struct 2017;164:32–42.
[17] Quang HL, He Q-C, Bonnet G. Eshelby's tensor fields and effective conductivity of composites made of anisotropic phases with Kapitza's interface thermal resistance. Phil Mag 2011;91(25):3358–92.
[18] Odegard G, Gates T, Wise K, Park C, Siochi E. Constitutive modeling of nanotube–reinforced polymer composites. Compos Sci Technol. 2003;63(11):1671–87.
[19] Sayers C. The elastic anisotrophy of shales. J Geophys Res Solid Earth 1994;99(B1):767–74.
[20] Johansen T, Jakobsen M, Ruud B. Estimation of the internal structure and anisotropy of shales from borehole data. J Seismic Explor 2002;11(4):363–82.
[21] Ulm F-J, Delafargue A, Constantinides G. Experimental microporomechanics. Applied Micromechanics of Porous Materials. Springer; 2005. p. 207–88.
[22] Lee JK, Kim K, Lee Y, Jeong T. Simultaneous intrinsic and extrinsic parameter identification of a hand-mounted laser-vision sensor. Sensors 2011;11(9):8751–68.
[23] Park HM, Park S, Lee S-M, Shon I-J, Jeon H, Yang B. Automated generation of carbon nanotube morphology in cement composite via data-driven approaches. Compos B Eng 2019;167:51–62.
[24] Jang J-u, Lee HS, Kim JW, Kim SY, Kim SH, Hwang I, et al. Facile and cost-effective strategy for fabrication of polyamide 6 wrapped multi-walled carbon nanotube via anionic melt polymerization of ε-caprolactam. Chem Eng J 2019;373:251–8.
[25] Jang J-u, Park HC, Lee HS, Khil M-S, Kim SY. Electrically and thermally conductive carbon fibre fabric reinforced polymer composites based on Nanocarbons and an in-situ Polymerizable cyclic Oligoester. Sci Rep 2018;8(1):7659.
[26] Yu J, Cha JE, Kim SY. Thermally conductive composite film filled with highly dispersed graphene nanoplatelets via solvent-free one-step fabrication. Compos B Eng 2017;110:171–7.
[27] Kim HS, Kim JH, Yang C-M, Kim SY. Synergistic enhancement of thermal conductivity in composites filled with expanded graphite and multi-walled carbon nanotube fillers via melt-compounding based on polymerizable low-viscosity oligomer matrix. J Alloys Compd 2017;690:274–80.
[28] Yang B, Hwang Y, Lee H. Elastoplastic modeling of polymeric composites containing randomly located nanoparticles with an interface effect. Compos Struct 2013;99:123–30.
[29] Harsch M, Karger-Kocsis J, Apostolov A. Crystallization-induced shrinkage, crystalline, and thermomechanical properties of in situ polymerized cyclic butylene terephthalate. J Appl Polym Sci 2008;108(3):1455–61.
[30] Noh YJ, Lee S, Kim SY, Youn JR. High-speed fabrication of thermoplastic carbon fiber fabric composites with a polymerizable, low-viscosity cyclic butylene terephthalate matrix for automotive applications. Macromol Res 2014;22(5):528–33.
[31] Ishak ZM, Gatos K, Karger-Kocsis J. On the in-situ polymerization of cyclic butylene terephthalate oligomers: DSC and rheological studies. Polym Eng Sci 2006;46(6):743–50.
[32] Wu D, Wu L, Yu G, Xu B, Zhang M. Crystallization and thermal behavior of multiwalled carbon nanotube/poly (butylenes terephthalate) composites. Polym Eng Sci 2008;48(6):1057–67.
[33] Jang HG, Yang B, Khil M-S, Kim SY, Kim J. Comprehensive study of effects of filler length on mechanical, electrical, and thermal properties of multi-walled carbon nanotube/polyamide 6 composites. Compos A Appl Sci Manuf 2019;125:105542.
[34] Haggenmueller R, Guthy C, Lukes JR, Fischer JE, Winey KI. Single wall carbon nanotube/polyethylene nanocomposites: thermal and electrical conductivity. Macromolecules 2007;40(7):2417–21.
[35] Yang K, Gu M, Guo Y, Pan X, Mu G. Effects of carbon nanotube functionalization on the mechanical and thermal properties of epoxy composites. Carbon 2009;47(7):1723–37.